Assessment of timberline boundary shift in the mountainous ecosystems of Subpolar Urals from multispectral satellite imagery over the last 40 years

Alexander Basmanov [1], Mikhail Bogachev [2], Andrey Grigoriev [3], Grigoriy Lozhkin [4], Denis Tishin [4]

[1] Dept. of Television and Video Systems, St. Petersburg Electrotechnical University, St. Petersburg, 197022, Russia – alex.basmanov00@gmail.com
[2] Radio Systems Dept., St. Petersburg Electrotechnical University, St. Petersburg, 197022, Russia – rogex@yandex.com
[3] Institute of Plant and Animal Ecology, Ural Brach of the Russian Academy of Sciences, Ekaterinburg, 620144, Russia – grigoriev.a.a@ipae.uran.ru
[4] Institute of Environmental Sciences, Kazan Federal University, Tatarstan, Kazan, 420008, Russia – kpfuecology@gmail.com

Keywords: Treeline, Timberline, Landsat, Mountain tundra, Boreal ecotone.

Abstract

Shifts in the habitat boundaries of woody plant species represent one of the continental-scale consequences of climate change. Mapping these shifts and quantitatively evaluating them is essential for an appropriate assessment of the carbon balance. Here we present a stepwise procedure including the selection and processing of multispectral remote sensing data from Landsat 4–9 on the Google Earth Engine servers. We show explicitly how these data can be used to assess the timberline boundary shift in the mountainous ecosystems of the Subpolar Urals (exemplified for the Sablya ridge) using such methods as pseudo–invariant feature matching, robust regression, principal component analysis, and logistic regression-based classification, resulting in high classification accuracy indicated by Intersection over Union (IoU) above 0.9. The quantitative evaluation of the overall forest advancement area from 1960 to 2024 — based on observations collected between 1987 and 2024 — was estimated at 4.82 km², in a reasonable agreement with the expert delineation estimate of 5.6 km².

1. Introduction

One of the consequences of ongoing climate change is the large–scale shift in ecological zone boundaries (Hansson et al., 2021; Montesano et al., 2024). In the Northern Hemisphere, the boundary of permafrost is retreating northwards, while arctic deserts are gradually being replaced by tundra. In particular, the southern boundary of the forest–tundra zone is progressively colonized by forest, thereby shifting the distribution limits of woody vegetation. Concurrently the southern edge of forested areas retreats under the influence of natural and anthropogenic factors detrimental to tree growth, including prolonged droughts, wildfires, and the intensification of agricultural practices. This retreat ultimately gives way to the establishment of steppe. Evaluating the balance between these divergent processes represents a complex and large-scale challenge, one that is also critical for a proper assessment of the carbon balance.

At the same time, mountain ecosystems serve as local models of global change. Typical of these regions is a division of the landscape into three primary zones: extensive areas devoid of forest but covered by herbaceous vegetation (e.g., cold rock deserts, stony debris fields, or wetlands); mountain tundra, characterized by the emergence of low-stature vegetation — mosses, lichens, herbaceous plants, small shrubs, and sporadic trees; and extensive forested areas (closed forest stands) (Gorchakovskiy and Shiyatov, 1985). Notably, these three zones are all subject to shifts under climatic forcing. For instance, mountain tundra gradually becomes colonized by woody vegetation — a process analogous to the northward shift of the southern continental boundary of forest–tundra zones (Harsch et al., 2009). Using mountain ecosystems as prominent examples, one can investigate processes comparable to those on a continental scale, yet restricted to small, locally defined study areas where several ecological zones may transition over distances of only a few hundred meters (as opposed to hundreds or thousands of kilometers on the plains) (Gorchakovskiy and Shiyatov, 1985). This scale-dependent heterogeneity facilitates the application of automated methods for analyzing and interpreting long-term Earth observation data, while still allowing for manual tuning, quality control, and cross-validation with expert assessments and local ground observations.

In modern conditions, remote sensing datasets from various sources enable the analysis of long-term changes in forest cover. Among these, multispectral Landsat data are of particular interest given their global scope and the continuity of their spatial and temporal coverage (Banskota et al., 2014). Moreover, state-of-the-art cloud computing tools and platforms now allow processing of massive remote sensing datasets without burdens such as data storage, database management, or extensive computational infrastructure (Hemati et al., 2021). This technological progress has allowed researchers to move from paired comparisons of multispectral images toward the automated analysis of time series that carry substantially more information — including the dynamics of ecological boundaries (Kennedy et al., 2010; Zhu and Woodcock, 2014; Huang et al., 2010).

2. Materials and Methods

The primary input data for this study consist of Landsat datasets and expert delineations of ecological zone boundaries obtained during field expeditions, as well as through the analyses of aerial photographs and satellite imagery. For the analysis, multispectral images from Landsat satellites 4 through 9 (second collection) (Crawford et al., 2023) acquired in July and August — available since 1984 for the study area — were

This contribution has been peer-reviewed.
https://doi.org/10.5194/isprs-archives-XLVIII-2-W9-2025-45-2025 | © Author(s) 2025. CC BY 4.0 License.

selected. The study area is defined as a square with 30-kilometer sides centered at the coordinates 59.05° E, 64.82° N. For some operations, an extended study area — a square measuring 90 kilometers on each side with the same center — was also employed (hereafter referred to as the extended area).

Cloud-free Tier 1 (T1) multispectral images of Top-Of-Atmosphere (TOA) reflectance that have undergone relative radiometric correction along with Surface Reflectance (SR) products were used in the analysis. The T1 data exhibits a Radial Root Mean Square Error (RMSE) of less than 12 meters between images, making them suitable for time-series analysis. All multispectral images include blue (B), green (G), red (R), near infrared (NIR), short-wave infrared (SWIR1 and SWIR2), and thermal bands that are common to all Landsat sensors. TOA images were used directly for assessing the boundary shift, whereas SR images served as auxiliary data during the classification stage. The exclusive use of SR products as supplemental information is motivated by inherent differences among sensors onboard Landsat 4–9. Time series constructed from SR images inevitably present trends in band brightness and in all derivative indices due to the gradual transition from older to newer sensor technologies. Therefore, relative radiometric correction — capable of mitigating sensor-transition effects — is more effectively executed from the base-level TOA data rather than by performing SR-to-SR correction. This is attributed to the fact that SR images already represent the outcome of an absolute radiometric correction; further relative correction these products would introduce additional error (Young et al., 2017).

Data processing was performed using Google Earth Engine (GEE), a cloud-based geospatial analysis platform that harnesses Google's computing capabilities and simplifies the processing of large remote sensing datasets (Gorelick et al., 2017). Within GEE, all operations related to individual image processing and time-series formation — including initial filtering, relative radiometric correction, and compositing — were executed. The time series were generated as sets of seasonal composite images, which were then exported from GEE for further local processing. The assessment of the forest boundary shift was carried out by performing a binary classification of pixels into forested and non-forested classes, followed by a temporal regression analysis of the resulting classifications.

2.1 Preliminary Filtering

The first step in processing the TOA data was to exclude all images that were more than one-quarter covered by dense clouds or semi-transparent haze in the extended area. To accomplish this, the Simple Cloud Score algorithm available on the Google Earth Engine (GEE) platform was applied to the images. This algorithm computes a cloud probability (in percentage) for each pixel of a multispectral Landsat TOA image using spectral brightness, temperature, and the Normalized Difference Snow Index (NDSI). Next, images for which the upper quartile of the cloud probability exceeded one percent were removed. This selection is justified by the fact that further relative radiometric correction may introduce substantial errors when applied to images with a high cloud load, and the early exclusion of such data accelerates the necessary calculations and transformations. On the remaining images, dilated clouds and their shadows were masked using the QA_PIXEL bit mask.

2.2 Relative Radiometric Correction

For the relative radiometric correction, a single TOA image (ID: LANDSAT/LE07/C02/T1_TOA/LE07_168015_20010717), which exhibits minimal cloud cover and the maximum overlap with the extended area, was chosen as the reference. Relative to this reference image, the remaining TOA images were corrected using the Pseudo-Invariant Feature Matching (PIF) method (Schroeder et al., 2006). This method is based on establishing a linear relationship between the spectral brightness of pseudo-invariant features on the reference image and their corresponding brightness on the image to be corrected. Pixels corresponding to pseudo-invariant features were determined by applying a similarity measure between spectral signatures using the Spectral Correlation Mapper (De Carvalho et al., 2013):

$$\mathrm{SCM} = \frac{\sum_{i=1}^{N}(P_i^{ref} - \bar{P}^{ref})(P_i - \bar{P})}{\sqrt{\sum_{i=1}^{N}(P_i^{ref} - \bar{P}^{ref})^2 \sum_{i=1}^{N}(P_i - \bar{P})^2}}, \quad (1)$$

where SCM = Spectral Correlation Mapper

P^{ref} = sample pixel from the reference image

$\bar{P}^{ref}$ = average brightness of the bands of the reference pixel

P = sample pixel from the image to be corrected

$\bar{P}$ = average brightness of the bands of the pixel from the image to be corrected

N = number of bands

i = band iterator

This measure represents the Pearson correlation coefficient computed on a pixel-by-pixel basis and enables the selection of those pixels with the highest linear correlation. The top 10% of the most correlated pixels were selected — independently in four brightness ranges defined by the quartiles and the median of each band of the reference image — by applying a logical OR condition, and pixels with a correlation below 0.8 were excluded. Using these selected pixels, the coefficients for linear transformation for each band were computed via robust linear regression employing iteratively reweighted least squares with the Talwar cost function. As a result, every spectral band of each TOA image was transformed according to the derived linear coefficients.

Thus, the relative radiometric correction was performed under the assumption that any TOA image intersecting with the reference image in the extended area contains enough spectrally similar pixels, the differences of which are attributable to variations in Landsat sensors, solar illumination angles, and atmospheric transparency — but not to phenological differences in vegetation (Young et al., 2017).

2.3 Compositing

After cloud removal and relative radiometric correction, the TOA images were merged into seasonal composites using the Normalized Difference Vegetation Index (NDVI):

$$\mathrm{NDVI} = \frac{\mathrm{NIR} - \mathrm{R}}{\mathrm{NIR} + \mathrm{R}}. \quad (2)$$

A composite was generated by selecting the pixel whose NDVI corresponded to the upper quartile of the seasonal distribution. This approach favors pixels near the seasonal peak of vegetation activity while excluding anomalous pixels whose high NDVI

values result from atmospheric effects rather than vegetation. In doing so, the composites become more consistent among themselves and further suppress any residual clouds and other anomalies. Seasonal composites of Surface Reflectance (SR) images were generated as median images for the period 2019–2024.

2.4 Expert Delineation of Ecological Zones

Expert delineations of ecological zones were obtained from field expeditions and through the expert analysis of multi-temporal aerial photographs and satellite imagery. In Figure 1, an example is shown where such delineations are visualized both as a closed boundary on a map and as a binary mask.

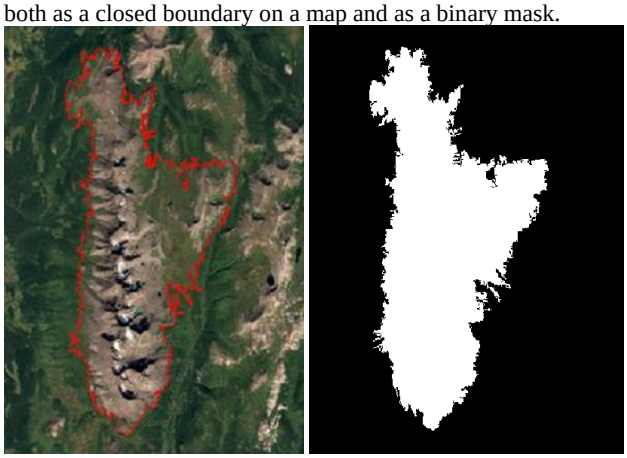

a b

Figure 1. Example of expert delineation of the boundary between mountain tundra and dense forest: (a) Closed boundary; (b) Binary mask.

Figure 2. Example of corrected binary mask

These expert delineations identify a set of pixels corresponding to non-forest areas, while the information regarding forest areas is used to generate training labels for subsequent classification into forest and non-forest classes. It is well established that, due to significant shadows cast by trees, forested areas generally appear darker than other vegetated surfaces, thereby producing a distinct “forest peak” in the histograms of certain spectral bands (Huang et al., 2008). Non-forest dark areas can be identified and masked using NDVI. Accordingly, the previously obtained SR composites were divided into square blocks of 200 pixels per side, and histograms for the G band and NDVI were computed for each block. Pixels considered to belong to forested areas were selected based on thresholds corresponding to the frequency peak in these histograms — specifically, by selecting pixels with NDVI above a set threshold and G values below a specified level. Figure 2 illustrates an example of the corrected binary mask obtained through the thresholding process, overlaid on a map. Blocks with a median NDVI below 0.8 were excluded, as these areas are less than half covered by dense vegetation and their histogram peaks are therefore unlikely to accurately represent closed forest stands. These outputs now serve directly as the training data for the subsequent classification of imagery into forest and non-forest areas.

2.5 Assessment of Timberline Boundary Shift

The assessment of the timberline boundary shift comprised two stages: classification of seasonal composites from the relative radiometrically corrected TOA images into forest and non-forest classes, and regression analysis of the classification results (i.e., the time series of decision statistics) to delineate the timberline boundary.

In the first stage, Principal Component Analysis (PCA) was applied to the B, G, R, and NIR bands, and the first two principal components (PC1 and PC2) were selected. The SWIR1 and SWIR2 bands, being moisture-dependent and not significantly enhancing the classification, were omitted. Training and classification were performed based on the features PC1, PC2, and NDVI — which, owing to its normalized nature, is independent of illumination and provides a straightforward means of partially mitigating illumination effects without resorting to a digital elevation model (Young et al., 2017). Corrected binary masks (a total of six masks spanning 2019–2024) were used as training labels for a logistic regression model, resulting in a time series of decision statistics from 1987 to 2024. In this way, forest and non-forest areas were clearly delineated, and the timberline boundary was defined as a transition zone between these areas. Classification quality was evaluated by comparing the predicted labels (obtained by binarizing the decision statistics using a threshold of 0.5) with the training labels via K-Fold Cross-Validation. For this purpose, the Intersection over Union (IoU) metric was employed:

$$\mathrm{IoU} = \frac{\mathrm{P} \cap \mathrm{GT}}{\mathrm{P} \cup \mathrm{GT}} = \frac{\mathrm{TP}}{\mathrm{TP} + \mathrm{FP} + \mathrm{FN}}, \quad (3)$$

where IoU = Intersection over Union
P = predicted class labels
GT = ground truth (training) labels
TP = True Positives
FP = False Positives
FN = False Negatives

The average IoU for the forest class was 0.9114 and 0.9371 for the non-forest class, yielding an overall average IoU of 0.9242. Figure 3 displays the ROC curves derived from cross-validation, with the area under the curves (AUC) averaging 0.9938. Regression analysis was then performed by applying linear regression individually to the decision statistic time series for each pixel to estimate the temporal movement of the timberline boundary.

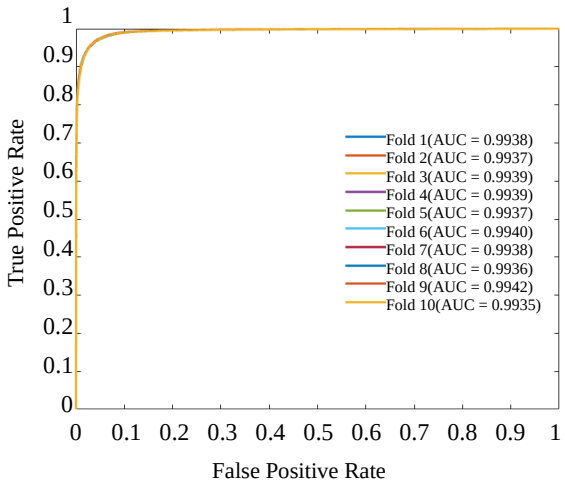

Figure 3. ROC curves derived from cross-validation

3. Results

Figure 4 visualizes the outcome of the linear regression applied to the time series. In the visualization, green is proportional to the mean value of the regression line, red indicates a negative derivative, and blue denotes a positive derivative. This map depicts long-term forest gain (blue) and forest loss (red) from 1987 to 2024. By extrapolating the regression to 1960 and binarizing the decision statistic time series at a threshold of 0.5, an estimated total forest advancement area of 4.82 km² was obtained for the expert-assessed vicinity of the Sablya ridge.

Figure 5 presents a graph showing the relationship between the forest advancement area and time, with red dots marking the start and end of the satellite observation period (1987 and 2024, respectively). The curve preceding 1987 results from extrapolation. From 1995 to 2024 the trend is linear; from 1970 to 1995, forest advancement occurred with an accelerating pace, while prior to 1970 the trend was linear. Dashed lines on the

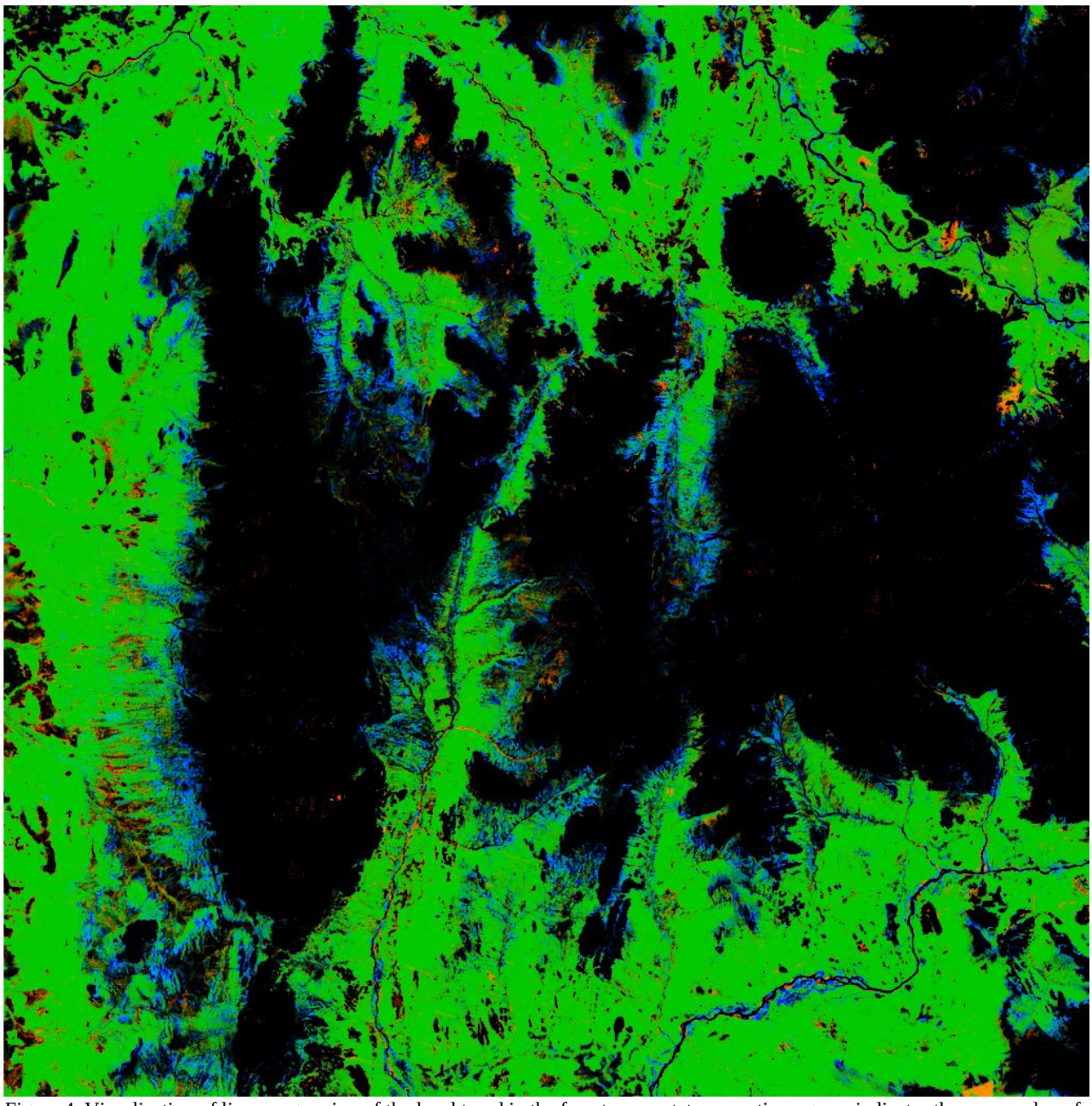

Figure 4. Visualization of linear regression of the local trend in the forest cover status over time: green indicates the mean value of the regression line, red indicates a negative derivative (forest loss), and blue indicates a positive derivative (forest gain)

graph indicate the approximations for these linear segments.

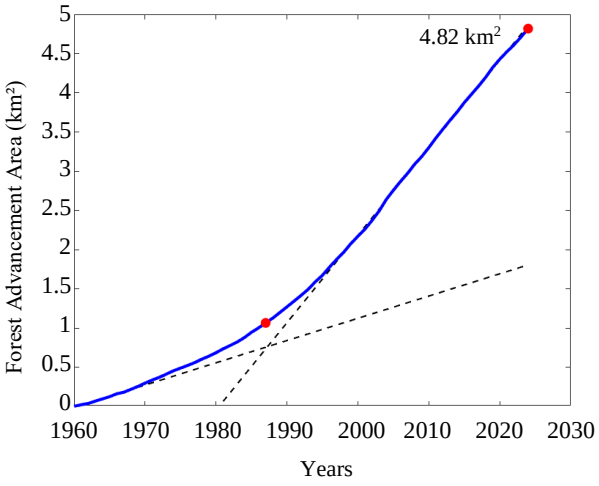

Figure 5. Evaluated forest advancement area time series

4. Conclusion

In the present study, the timberline boundary shift was assessed using multispectral Landsat 4–9 images and expert evaluations of ecological zone boundaries in the mountain ecosystem of the Sablia ridge in the Subpolar Urals. Based on the decision statistic time series from 1987 to 2024, a map delineating forest gain and forest loss was produced. The map shows that forest gain is concentrated near the mountains — an expected upward shift of the forest edge under the influence of observed climate change. Although some forest loss is evident, these losses are distributed more randomly and uniformly across the study area. The assessment of the timberline boundary shift — extrapolated from the decision statistic time series — yields an advancement area of 4.82 km² from 1960 to 2024, while expert evaluations for the same period and area indicate an advancement of 5.6 km². These results are considered consistent, given the spatial resolution constraints of Landsat 4–9 (30 m) and the fact that approximately 30% of the expert-documented forest advancement involves shifts smaller than this resolution. The relationship between forest advancement area and time exhibits an inflection between 1970 and 1995, which aligns with climatic meta-analysis data indicating a significant pivot in temperature trends in the late 1980s (Reid et al., 2016). Conversely, linear extrapolation captures only trends observed during the study period and omits pre-observation dynamics. This limitation may affect the curve's shape, though likely only marginally due to the very slow and protracted processes occurring in the mountain ecosystems of the Subpolar Urals.

The use of the GEE platform allowed the most resource-intensive operations to be offloaded to Google's servers, rapidly condensing large volumes of long-term remote sensing data into compact seasonal composite time series that can be easily exported and processed locally. This setup not only mitigates many challenges associated with local processing of big data but also significantly streamlines and accelerates experiments in other regions.

The results presented here can serve as a foundation for more advanced mathematical models of forest cover change and timberline dynamics. For instance, a more effective approach to capturing the temporal dynamics of forest advancement may involve piecewise-linear approximation of the decision statistic time series. A notable example of such an approach is the LandTrendr temporal segmentation algorithm (Kennedy et al., 2010). In regions with climates more favorable to vegetation than the high mountains of the Subpolar Urals — and in areas affected by fire or other anthropogenic disturbances — piecewise-linear approximation can effectively accommodate abrupt and nonlinear changes in forest cover. Additionally, the use of optical flow methods holds promise for developing predictive models of timberline movement.

Acknowledgements

We like to acknowledge the financial support of this work by the Ministry of Science and Higher Education of the Russian Federation in the framework of assignment FSEE-2025-0006.

References

Banskota, A., Kayastha, N., Falkowski, M.J., Wulder, M.A., Froese, R.E., & White, J.C. (2014). Forest Monitoring Using Landsat Time Series Data: A Review. *Canadian Journal of Remote Sensing*, 40(5), 362–384. doi:10.1080/07038992.2014.987376

Crawford, C.J., Roy, D.P., Arab, S., Barnes, C., Vermote, E., Hulley, G., Gerace, A., Choate, M., Engebretson, C., Micijevic, E., Schmidt, G., Anderson, C., Anderson, M., Bouchard, M., Cook, B., Dittmeier, R., Howard, D., Jenkerson, C., Kim, M., Kleyians, T., Maiersperger, T., Mueller, C., Neigh, C., Owen, L., Page, B., Pahlevan, N., Rengarajan, R., Roger, J.-C., Sayler, K., Scaramuzza, P., Skakun, S., Yan, L., Zhang, H.K., Zhu, Z., & Zahn, S. (2023). The 50-year Landsat Collection 2 Archive. *Science of Remote Sensing*, 8, Article 100103. doi:10.1016/j.srs.2023.100103

De Carvalho, O.A., Guimarães, R.F., Silva, N.C., Gillespie, A.R., Gomes, R.A.T., Silva, C.R., & De Carvalho, A.P.F. (2013). Radiometric Normalization of Temporal Images Combining Automatic Detection of Pseudo-Invariant Features from the Distance and Similarity Spectral Measures, Density Scatterplot Analysis, and Robust Regression. *Remote Sensing*, 5(6), 2763–2794. doi:10.3390/rs5062763

Gorchakovskiy, P.L., & Shiyatov, S.G. (1985). Fitoindikatsiya usloviy sredy i prirodnykh protsessov v vysokogor'yakh [Phytoindication of Environmental Conditions and Natural Processes in the Highlands]. Moscow: *Nauka (Science)*. (In Russ.)

Gorelick, N., Hancher, M., Dixon, M., Ilyushchenko, S., Thau, D., & Moore, R. (2017). Google Earth Engine: Planetary-Scale Geospatial Analysis for Everyone. *Remote Sensing of Environment*, 202, 18–27. doi:10.1016/j.rse.2017.06.031

Hansson, A., Dargusch, P., & Shulmeister, J. (2021). A Review of Modern Treeline Migration, the Factors Controlling It and the Implications for Carbon Storage. *Journal of Mountain Science*, 18, 291–306. doi:10.1007/s11629-020-6221-1

Harsch, M.A., Hulme, P.E., McGlone, M.S., & Duncan, R.P. (2009). Are Treelines Advancing? A Global Meta-Analysis of Treeline Response to Climate Warming. *Ecology Letters*, 12(10), 1040–1049. doi:10.1111/j.1461-0248.2009.01355.x

Hemati, M., Hasanlou, M., Mahdianpari, M., & Mohammadimanesh, F. (2021). A Systematic Review of

Landsat Data for Change Detection Applications: 50 Years of Monitoring the Earth. *Remote Sensing*, 13(15), Article 2869. doi:10.3390/rs13152869

Huang, C., Song, K., Kim, S., Townshend, J.R.G., Davis, P., Masek, J.G., & Goward, S.N. (2008). Use of a Dark Object Concept and Support Vector Machines to Automate Forest Cover Change Analysis. *Remote Sensing of Environment*, 112(3), 970–985. doi:10.1016/j.rse.2007.07.023

Huang, C., Goward, S.N., Masek, J.G., Thomas, N., Zhu, Z., & Vogelmann, J.E. (2010). An Automated Approach for Reconstructing Recent Forest Disturbance History Using Dense Landsat Time Series Stacks. *Remote Sensing of Environment*, 114(1), 183–198. doi:10.1016/j.rse.2009.08.017

Kennedy, R.E., Yang, Z., & Cohen, W.B. (2010). Detecting Trends in Forest Disturbance and Recovery Using Yearly Landsat Time Series: 1. LandTrendr — Temporal Segmentation Algorithms. *Remote Sensing of Environment*, 114(12), 2897–2910. doi:10.1016/j.rse.2010.07.008

Montesano, P., Frost, M., Li, J., Carroll, M., Neigh, C., Macander, M., Sexton, J., & Frost, G. (2024). A Shift in Transitional Forests of the North American Boreal Will Persist Through 2100. *Communications Earth & Environment*, 5, Article 290. doi:10.1038/s43247-024-01454-z

Reid, P.C., Hari, R.E., Beaugrand, G., Livingstone, D.M., Marty, C., Straile, D., Barichivich, J., Goberville, E., Adrian, R., Aono, Y., Brown, R., Foster, J., Groisman, P., Hélaouët, P., Hsu, H.-H., Kirby, R., Knight, J., Kraberg, A., Li, J., Lo, T.-T., Myneni, R.B., North, R.P., Pounds, J.A., Sparks, T., Stübi, R., Tian, Y., Wiltshire, K.H., Xiao, D., & Zhu, Z. (2016). Global Impacts of the 1980s Regime Shift. *Global Change Biology*, 22(2), 682–703. doi:10.1111/gcb.13106

Schroeder, T., Cohen, W., Song, C., Canty, M., & Yang, Z. (2006). Radiometric Correction of Multi-Temporal Landsat Data for Characterization of Early Successional Forest Patterns in Western Oregon. *Remote Sensing of Environment*, 103, 16–26. doi:10.1016/j.rse.2006.03.008

Young, N., Anderson, R., Chignell, S., Vorster, A., Lawrence, R., & Evangelista, P. (2017). A Survival Guide to Landsat Preprocessing. *Ecology*, 98, 920–932. doi:10.1002/ecy.1730

Zhu, Z., & Woodcock, C.E. (2014). Continuous Change Detection and Classification of Land Cover Using All Available Landsat Data. *Remote Sensing of Environment*, 144, 152–171. doi:10.1016/j.rse.2014.01.011